

# Monitoring of the Plasmon Resonance of Gold Nanoparticles in Au/TiO<sub>2</sub> Catalyst under Oxidative and Reducing Atmospheres

Y. Borensztein,<sup>\*,†</sup> L. Delannoy,<sup>‡</sup> A. Djedidi,<sup>†</sup> R. G. Barrera,<sup>§</sup> and C. Louis<sup>‡</sup>

*Institut des NanoSciences de Paris, CNRS and UPMC University of Paris 06, UMR 7588, 140, rue de Lourmel, 75015 Paris, France, Laboratoire de Réactivité de Surface, CNRS and UPMC University of Paris 06, UMR 7197, 4 place Jussieu, 75252 Paris cedex 05, France, and Instituto de Fisica, Universidad Nacional Autonoma de Mexico, Mexico D.F., Mexico*

*Received: February 9, 2010; Revised Manuscript Received: April 7, 2010*

Diffuse optical reflectance of Au/TiO<sub>2</sub> powder catalysts, prepared by the deposition–precipitation method, is measured in the UV–visible range in controlled atmosphere. An intense optical absorption observed around 550 nm is interpreted by the excitation of plasmon resonances in the 4 nm gold nanoparticles (NPs). The location, intensity, and width of the absorption can be reproduced theoretically by using a distribution of shapes of the NPs. The changes of the reflectance upon exposure of the Au/TiO<sub>2</sub> catalyst to different atmospheres (O<sub>2</sub>/He, H<sub>2</sub>/He, CO/He) are measured in real-time by use of a homemade differential diffuse reflectance (DDR) spectrometer. The derivative-like DDR spectrum shows that the exposure to oxygen leads to the adsorption of oxygen species at the surface of the Au NPs. By modeling the DDR spectrum, we analyze different possible processes that could occur during the oxygen exposure and we find that the main effect is a charge transfer from gold to the adsorbed oxygen species, combined with a slight flattening of the Au NPs. The exposure to CO gives a similar but much smaller effect than the one of oxygen. Finally, real-time optical measurements performed during the exposures to oxygen indicate that two different sets of particles are probably present in the catalyst, and react with different kinetics, slightly flat three-dimensional NPs and very flat almost two-dimensional NPs.

## 1. Introduction

Contrarily to bulk gold which is essentially inert, it has been demonstrated that supported gold nanoparticles (NPs) can have remarkable catalytic properties in a wide range of oxidation and hydrogenation reactions, and especially in the CO oxidation reaction at low temperature.<sup>1</sup> The mechanism of this latter reaction is still unclear.<sup>2,3</sup> While it is largely accepted that CO adsorbs on the low coordination surface sites of the gold nanoparticles,<sup>4</sup> the important issue of the O<sub>2</sub> activation is still very much controversial.<sup>5–13</sup> It has been proposed that oxygen could directly react with gold.<sup>6,12,14</sup> The possible role of the NPs-support interface, or of the sites at the perimeter of the Au NPs, has also been pointed out to explain the oxygen activation.<sup>7,11,15–17</sup> The role of the substrate is indeed very important. Most of the works report that gold nanoparticles supported on reducible oxide supports are more active than gold on nonreducible supports. However, some studies also report catalytic activity when gold is supported on nonreducible support, which would mean that oxygen could interact with gold on which CO is adsorbed. The existence of interaction between molecular oxygen species and gold particles in Au/TiO<sub>2</sub> model catalysts has been proposed<sup>18–20</sup> and oxidation of surface gold atoms on gold nanoparticles has been shown.<sup>9,21,22</sup> A study by extended X-ray absorption fine structure spectroscopy (EXAFS)<sup>21</sup> revealed indeed the presence of oxygen atoms in the local environment of gold atoms of small gold particles, when supported gold

catalysts were put in air after a reducing treatment. X-ray absorption near-edge spectroscopy (XANES) studies<sup>9,10,23</sup> revealed charge transfer between gold nanoparticles and adsorbed CO and oxygen species. Finally, environmental high-resolution transmission electron microscopy (E-HRTEM), working at 2 mbar, showed that the shape of Au nanoparticles slightly changes in the presence of a gas, displaying facets under hydrogen or under vacuum and becoming rounded under oxygen.<sup>12</sup> These results are also strong indications of direct adsorption of oxygen species on the Au nanoparticles. In contrast with these results, a very recent ambient-pressure X-ray photoemission spectroscopy (AP-XPS) investigation by Salmeron et al. showed that Au NPs obtained by evaporation onto the TiO<sub>2</sub>(110) surface could not be oxidized at pressures up to 1 Torr of oxygen, except under X-ray radiation.<sup>13</sup>

The UV–visible spectroscopy is one of the few “operando” methods that can be used to in situ investigate the modifications of the physical or chemical properties of catalysts during exposure to gases or during catalytical reactions; in contrast with AP-XPS and E-HRTEM, it can be used at atmospheric pressure, or even at higher pressure. If oxygen interacts with Au particles, specific effects are expected, such as change of particle shape or charge transfer, that should be detected by optical measurements. We have developed an original experimental method to perform real-time studies of the optical response of working catalysts during their exposure to gas at atmospheric pressure. In this study, the catalyst is a powder consisting of gold nanoparticles supported on TiO<sub>2</sub> crystallites, which display large diffuse reflectance spectra, with features interpreted in terms of the excitation of the plasmon resonance (PR) of the gold nanoparticles (NPs) by the incident light.

\* To whom correspondence should be addressed. E-mail: yves.borensztein@insp.upmc.fr.

<sup>†</sup> CNRS and UPMC University of Paris 06, UMR 7588.

<sup>‡</sup> CNRS and UPMC University of Paris 06, UMR 7197.

<sup>§</sup> Universidad Nacional Autonoma de Mexico.

The purpose of this work is to correlate the changes of diffuse reflectance, that is, the changes of the optical properties of the Au/TiO<sub>2</sub> catalyst when the gas atmosphere is switched for instance from H<sub>2</sub> to O<sub>2</sub> or vice versa with changes in the physical and chemical properties of the catalyst. To achieve this goal, the diffuse reflectance spectra are modeled according to various hypotheses regarding the chemical properties of gold (resulting from changes in the oxidation state of gold or the possible charge transfer between Au and adsorbed entities), and the geometrical properties of the sample such as the shape of the gold particles. Moreover, the time resolution of this technique, of the order of one second, enables also kinetic studies during adsorption or desorption of a gas.

## 2. Experimental Section

### 2.1. Au/TiO<sub>2</sub> Catalyst Preparation and Characterization.

The catalysts were prepared by deposition–precipitation with urea (DP Urea) as described previously using TiO<sub>2</sub> (P25, Degussa, 50 m<sup>2</sup>/g, 70% anatase, 30% rutile) as support.<sup>24,25</sup> Typically, a solution of HAuCl<sub>4</sub> (300 mL, 2 × 10<sup>-3</sup> M) corresponding to the desired gold loading (4 wt %, that is, 0.8% in volume with respect to the volume of TiO<sub>2</sub>) was prepared by dissolving the appropriate amount of HAuCl<sub>4</sub>·3H<sub>2</sub>O in distilled water. Urea was added to the gold solution (C<sub>urea</sub> ~ 100 × C<sub>Au</sub>). The support material (3 g) was added and the suspension was stirred and heated to 80 °C for 16 h in a dark, closed reactor. The obtained solid was separated by centrifugation, washed three times with distilled water (with centrifugation between each washing) and dried under vacuum at room temperature for 12 h, resulting in the “as-prepared” samples. The final catalyst was obtained after activation under air (calcination) at 500 °C (2 °C/min from RT to 500 °C then 2 h at the final temperature). It has been previously shown that such a calcination treatment resulted in the formation of metallic gold nanoparticles with size below 5 nm supported on the titania particles.<sup>26</sup>

TEM analysis was performed using a JEOL 100 CX II microscope. The histograms of the metal particle sizes were established from the measurement of 300 particles. The size limit for the detection of gold particles on these supports is about 1 nm.

**2.2. Optical Measurements.** Two kinds of optical measurements were done. Before studying the relative changes of the diffuse reflectance induced by exposure to gas, the determination of the absolute reflectance of the catalyst is needed. For this purpose, we first performed absolute diffuse reflectance measurements, by using a commercial spectrophotometer (Cary 5) equipped with an integrating sphere after calibration with a PTFE white reference. The powder samples were placed in a sample holder, whose depth was large enough for the powder sample to be opaque. Since this apparatus measured the signal “wavelength after wavelength” by use of a monochromator, it did not allow us to perform spectral kinetic measurements; moreover, due to its geometry, the sample was in ambient air and measurements in a controlled atmosphere were not possible.

Second, in order to monitor in real time the changes of the diffuse reflectance induced by exposure to gas, we used another equipment with a simpler geometry, a home-developed differential diffuse reflectance spectrometer (DDRS), whose scheme is shown in Figure 1. The catalyst sample was placed in a home-built cell with a fused quartz window. A constant gas flow was maintained (either pure He, or He with fractions of different gas, that is, H<sub>2</sub>, O<sub>2</sub>, and CO). Light impinged the sample from an optical fiber at an angle of incidence of 45° with respect to

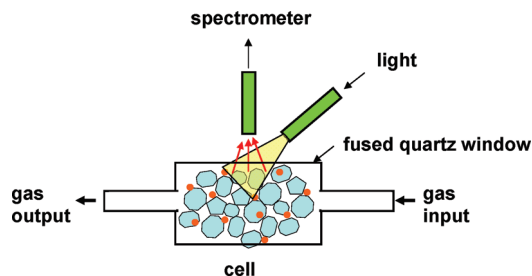


Figure 1. Scheme of the differential diffuse reflectance spectrometer.

the window of the cell, and the scattered light was collected with a second optical fiber normal to the window; this configuration allowed us to eliminate the specular reflection of the window and to collect only the diffuse light coming from the powder sample. Given this experimental setup, the measured quantity is the differential change of the diffuse reflectance between two states 1 and 2 of the sample, for example, under two different gaseous atmospheres, and defined as

$$\frac{\Delta R}{R} = \frac{R_2 - R_1}{R_1} \quad (1)$$

The spectrometer relied on a CCD camera, which delivered the reflectance spectra over the whole spectral range in a few milliseconds, and then integrated the received signal during 0.5 to 2 s to increase the signal/noise ratio. This enabled us to follow the change of reflectance of the sample in real time, during exposure to gas, and to investigate the kinetics of gas-induced changes (adsorption, reaction, etc.). As it will be seen by the experimental results presented below, this differential technique is extremely sensitive and allows one to detect very small changes of the catalyst. To avoid spurious effects coming from possible photochemical properties of TiO<sub>2</sub> when illuminated by ultraviolet light, we used a high-pass filter to eliminate light with wavelength below 390 nm, which corresponds to the absorption edge of TiO<sub>2</sub>. All the measurements were performed at room temperature and at atmospheric pressure. The flow rate of the ultrapure gases (99.999%) introduced in the cell was fixed to a total value of 25 mL/min with the following values: (i) pure He, 25 mL/min; (ii) O<sub>2</sub> in He, 2.5 and 22.5 mL/min, respectively; H<sub>2</sub> in He, 5 and 20 mL/min; CO in He, 1 and 24 mL/min.

## 3. Results

### 3.1. Transmission Electron Microscopy (TEM) Results.

Former studies<sup>26</sup> showed that Au<sup>III</sup> precursor present in Au/TiO<sub>2</sub> samples after deposition-precipitation is reduced to Au<sup>0</sup> after calcination at 500 °C. Figure 2A shows a transmission electron micrograph (TEM) of the calcined Au/TiO<sub>2</sub> catalyst measured in high vacuum. The light gray large particles with an average size around 20–30 nm, are the TiO<sub>2</sub> crystallites, while the dark gray small particles are the gold nanoparticles (Au NPs). The size histogram of the gold particles in Figure 2B shows a Gaussian-like distribution. The average size of the NPs is 4 nm and the standard deviation is around 1.4 nm. Moreover, it can be seen in the micrograph that some NPs appear to be somehow flattened (circled on the figure), but the resolution and the statistics are not good enough to give a quantitative determination of the proportion of flattened particles and the extent of flattening. Nevertheless, this is in agreement with former high-resolution TEM studies of Au/TiO<sub>2</sub> samples prepared by the

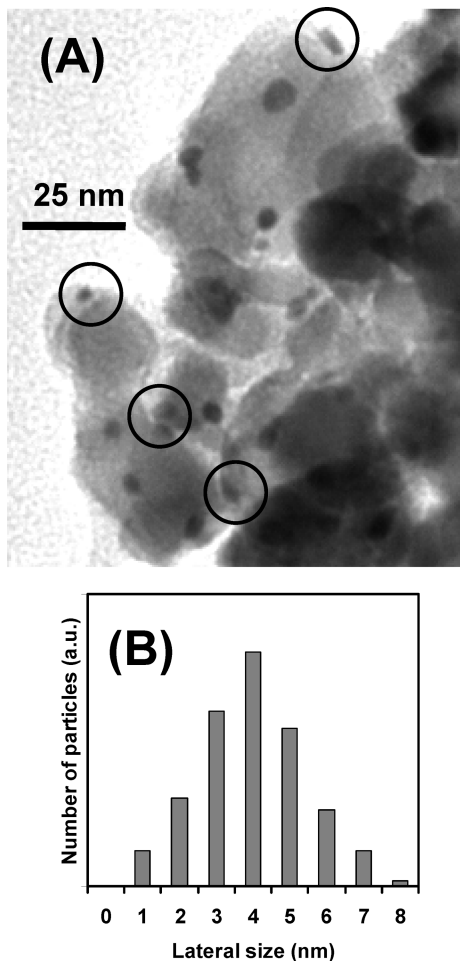


**Figure 2.** (A) Transmission electron micrograph of the Au/TiO<sub>2</sub> catalyst (110 nm × 130 nm). (B) Distribution of size of the Au NPs.

same method, which showed flattened particles with a truncated cuboctahedron shape.<sup>26</sup>

**3.2. Absolute Diffuse Reflectance Measurements.** Since the main purpose of this article is to relate the changes of diffuse reflectance, measured on the sample during gas adsorption, with the physical and chemical modifications of the catalyst, we first characterized the catalyst without any gas adsorption to correlate the physicochemical and geometrical properties of its constituents to the absolute diffuse reflectance. The calcined Au/TiO<sub>2</sub> catalyst under a H<sub>2</sub>/He gas mixture at room temperature is expected to be constituted by metallic Au<sup>0</sup> particles supported on the TiO<sub>2</sub> grains. On the contrary, when the catalyst is placed in air (or in O<sub>2</sub>/He), it is expected to end up in a somehow “oxidized” state with possible changes in particle morphology. However, as explained above, the absolute diffuse reflectance measurements could only be performed with the sample maintained in air. Consequently, we first present the measurement in air. Then, by using the differential diffuse reflectance measurements, we derive the absolute diffuse reflectance of the sample in H<sub>2</sub>, that is, in its reduced state. Finally, we develop a theoretical model to relate the diffuse reflectance with the morphological parameters describing the catalyst that enables us to obtain the distribution of shapes of the Au NPs. As discussed below, the distribution of size shown in Figure 2B has very little influence on the optical properties of the Au NPs.

**a. Au/TiO<sub>2</sub> Exposed to Air.** The absolute diffuse reflectance spectra of both the calcined TiO<sub>2</sub> and Au/TiO<sub>2</sub> samples were first recorded in air by using the Cary spectrophotometer equipped with the integrating sphere (Figure 3). The reflectance

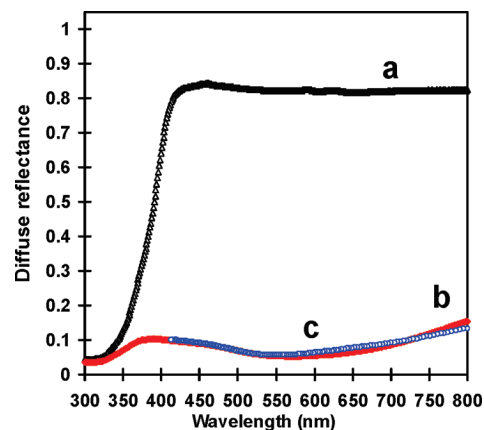


**Figure 3.** Experimental absolute diffuse reflectance. (a) Black empty triangles, TiO<sub>2</sub> powder in air; (b) Red-filled dots, Au/TiO<sub>2</sub> powder in air; (c) blue empty dots, Au/TiO<sub>2</sub> powder in hydrogen.

measured on the TiO<sub>2</sub> powder (curve a) is very high between 400 and 800 nm with no spectral features; this indicates that the TiO<sub>2</sub> particles scatter light very efficiently with extremely small absorption in this spectral range. Below 400 nm, the reflectance drastically drops, because of the rise of the intrinsic absorption of TiO<sub>2</sub>, due to interband transitions in rutile and anatase grains induced by light. In comparison, the diffuse reflectance of Au/TiO<sub>2</sub> (curve b) drops remarkably in all the spectral range. This strong decrease in the diffuse reflectance spectrum of the sample is therefore related to the optical absorption of light by the Au NPs and can be attributed to the excitation of the plasmon resonance (PR) in the Au nanoparticles.

To see more clearly this absorption, we used in the following the simple two-flux approximation of radiation transfer theory, that is, the Kubelka–Munk theory.<sup>27,28</sup> The radiation transfer theory is based essentially on flux conservation and, in the two-flux approximation, one considers that the diffuse field travels, on the average, only in the two opposite directions perpendicular to the interfaces of a slab-shaped sample. In this approximation, there are two phenomenological parameters, usually denoted by *S* and *K*, which are measures of the strengths of the scattering and of the absorption of the constituent particles within an element of volume, respectively. It is generally accepted that the two-flux approximation is valid for systems where scattering is large and absorption is low. In the case of thick-enough samples (that is, opaque), which is our case, the relationship between the diffuse reflectance *R* and the phenomenological parameters *K* and *S* becomes a function of only one parameter, *K/S*, and it is given by

$$R = 1 + \frac{K}{S} - \sqrt{\left(1 + \frac{K}{S}\right)^2 - 1} \quad \text{or} \quad \frac{K}{S} = \frac{(1 - R)^2}{2R} \quad (2)$$

where *R* is the diffuse reflectance. From the reflectance measurements of TiO<sub>2</sub> and of Au/TiO<sub>2</sub> exposed to air (cf. Figure 3), the *K/S* ratios are derived by use of eq 2 and the spectra are drawn in Figure 4.<sup>29</sup> For the TiO<sub>2</sub> sample (without Au NPs, spectrum a), the absorption due to the interband transitions starts at wavelength below 400 nm. For Au/TiO<sub>2</sub> (spectrum b), the strong absorption centered at 570 nm and with a width of about 200 nm is typical of the plasmon resonance (PR) in the Au nanoparticles whose location and shape depend generally on the size, on the shape of the Au nanoparticles, and on their environment.<sup>30,31</sup>

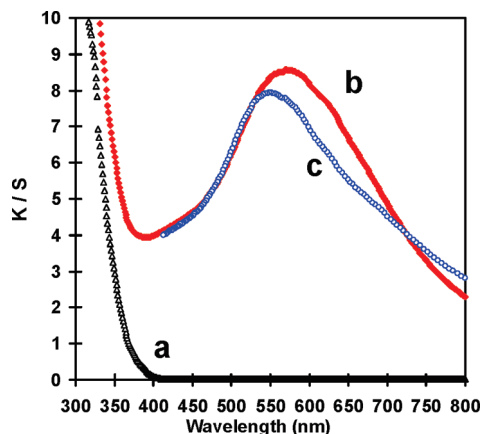


**Figure 4.** Experimental  $K/S$  derived from the diffuse reflectance spectra of Figure 3. (a) Black empty triangles, TiO<sub>2</sub> powder in air; (b) red-filled dots, Au/TiO<sub>2</sub> powder in air; (c) blue empty dots, Au/TiO<sub>2</sub> powder in hydrogen.

**b. Au/TiO<sub>2</sub> Exposed to H<sub>2</sub>.** As mentioned above, the experimental setup used above did not enable us to perform direct measurement of absolute diffuse reflectance of the samples under controlled atmosphere and, for instance, under H<sub>2</sub> ( $R_{H_2}$ ). We solved this problem as follows. After the determination of the absolute diffuse reflectance  $R_{air}$  of Au/TiO<sub>2</sub> exposed to air, as shown above, we performed the differential measurement  $(R_{O_2} - R_{H_2})/(R_{H_2})$  with the home-developed cell in our DDRS apparatus (see next section and Figure 6); from these measurements, and assuming that the diffuse reflectance of the sample is identical in air and in controlled O<sub>2</sub> atmosphere, we obtained  $R_{H_2}$ . The validity of this procedure is because the light reflected diffusely by the powder is quasi isotropic; hence no relevant differences in differential measurements are expected when the diffused light is collected by use of the integrating sphere of the CARY, or by use of the output fiber of the DDRS. The so-obtained absolute reflectance spectrum  $R_{H_2}$  is drawn in Figure 3 (spectrum c) and displays only very small differences with respect to the spectrum measured in air. The corresponding spectrum  $K/S$  for hydrogen environment is also drawn in Figure 4 (spectrum c). Compared to the one obtained in air (spectrum b), the PR is blue shifted with its maximum located at 550 nm and a smaller width of about 180 nm, but displays a slightly higher tail, that is, a higher absorption, for long wavelengths. In contrast, in the case of the pure TiO<sub>2</sub> sample no change is observed when the sample is exposed to H<sub>2</sub> instead of air (not reported in the figure).

**c. Determination of the Distribution of Shapes of the Au NPs.** To our knowledge, no calculation of the plasmon absorption spectrum has been attempted for supported gold particles with different realistic faceted shapes. In a recent publication, Gonzalez et al.<sup>32</sup> have shown that in the case of unsupported elongated prisms, the absorption band is dominated by a long wavelength resonance along the long axis, which is similar both in location and in width to the one of a prolate spheroid. In our case, we deal with flat particles. Thus, we can expect that the resonance at long wavelength that appears in the absorption spectrum of a flat spheroid could represent properly the main features of the absorption spectrum of flat-faceted particles. Moreover, since we most likely have a distribution of shapes, the exact location of this long wavelength resonance will not be critical. We now proceed to the determination of the distribution of shapes of the reduced Au NPs. To do this, we first regard the NPs as supported oblate spheroids with the revolution axis perpendicular to the surface of the TiO<sub>2</sub> substrate,

and then we fit the absolute diffuse reflectance spectrum of the sample in hydrogen (Figures 3 and 4, spectra c). This result will be the basis of the analysis of the diffuse differential reflectance spectra presented in the next paragraph, where we will propose modifications of the so-determined morphological properties and/or of the electronic properties of the catalyst when the sample is exposed to other gases.

In this paragraph, we first derive the formulas to relate the absolute diffuse reflectance  $R_{H_2}$  of the reduced sample, to the composition and morphological parameters of the catalyst. Second, we determine the distribution of shapes of the Au NPs that enables us to fit the experimental data. For gold particles much smaller than the wavelength of light, which is the case here since they have an average size of 4 nm, it is well-known that the plasmon resonance is of dipolar-type and does not depend on the size.<sup>33–36</sup> In the case of spherical particles, the resonance is obtained for  $\text{Re}(\epsilon_{Au}/\epsilon_m) = -2$ , where  $\epsilon_{Au}$  and  $\epsilon_m$  are the complex dielectric functions of gold and of the embedding medium, respectively, and  $\text{Re}$  denotes the real part. Using the dielectric function of bulk gold,<sup>37</sup> the resonance is located at  $\lambda_{PR} = 506$  nm for Au nanospheres isolated in a gas (with  $\epsilon_m = 1$ ). The absorption peak shifts to longer wavelength (red shift) when the surrounding medium is a nonabsorbing dielectric medium with an index of refraction larger than 1 (e.g.,  $\lambda_{PR} = 523$  nm for water with  $n_{water} = (\epsilon_{water})^{1/2} = 1.33$ ,  $\lambda_{PR} = 535$  nm for glass with  $n_{glass} = (\epsilon_{glass})^{1/2} = 1.50$ , and  $\lambda_{PR} = 633$  nm for anatase with  $n_{anatase} = (\epsilon_{anatase})^{1/2} = 2.4$ ). For supported gold particles, the situation is intermediate between isolated particles and embedded ones, and the interaction with the substrate also induces a red shift of the absorption resonance,<sup>38</sup> together with the excitation of additional multipolar resonances.<sup>39,40</sup> On the other hand, possible quantum size effect leading to the spill out of the free electron distribution at the surface might be important for particles smaller than 4 nm.<sup>35,41,42</sup> Such effect can give a blue shift of the resonance, as large as  $\Delta\lambda = 40$  nm for particles as small as 2 nm. In addition, if the supported Au NPs are not spherical, which seems to be the case for some of them in the present sample, at least under high vacuum (Figure 2), the absorption resonance is expected to be split into several resonances (three dipolar resonances for an ellipsoidal shape, two for a spheroidal shape, and several multipolar resonances for nonellipsoidal shapes).<sup>30</sup> Because of the large width of the gold plasmon resonance band, these splittings should appear as a shift and a broadening of the resonance. The observed resonance in  $K/S$  (curve c of Figure 4 and drawn again in Figure 5A) is red shifted and much broader than the one of a single Au sphere supported on TiO<sub>2</sub>, whose width is about 100 nm (theoretical curve (1') drawn in Figure 5A with dashed line). This broadening of the PR can originate from both intrinsic and extrinsic (that is, inhomogeneous) broadenings. The intrinsic broadening in a single particle can have several causes, the decrease of the mean free path of the conduction electrons due to the scattering from the surface, the splitting of the dipolar plasmon resonance, and the excitation of multipolar resonances. The inhomogeneous broadening is due to a collection of particles with different shapes, displaying resonances at different positions.

To reproduce the experimental spectrum, we calculated the  $K/S$  curves for different shapes of the oblate spheroidal particles supported on the TiO<sub>2</sub>. Since both TiO<sub>2</sub> grains and Au NPs can absorb and scatter light, the quantities  $K$  and  $S$  can be written as

$$K = K_{Au} + K_{TiO_2} \quad \text{and} \quad S = S_{Au} + S_{TiO_2} \quad (3)$$

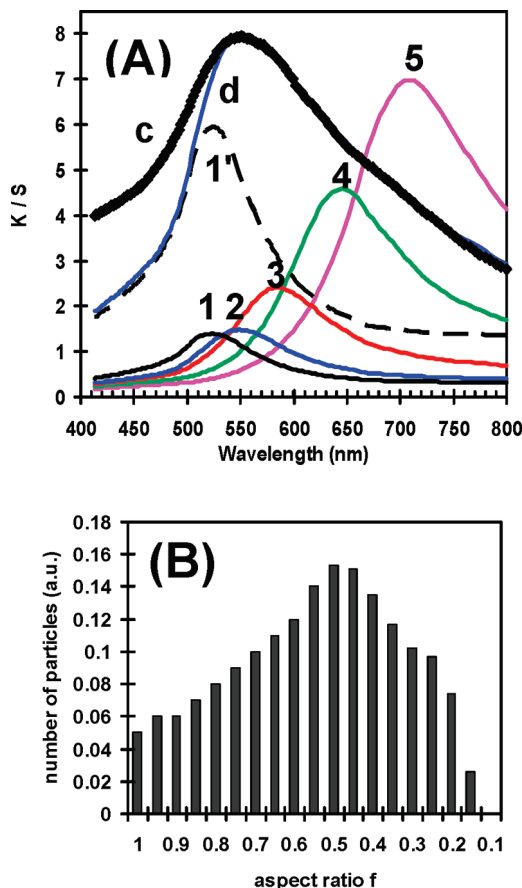


**Figure 5.** (A) (c) Experimental  $K/S$  derived from the diffuse reflectance spectrum of Au/TiO<sub>2</sub> under hydrogen (black dots). Numbered color curves: calculated  $K/S$  for different shapes, (1)  $f = 1$ ; (2)  $f = 0.45$ ; (3)  $f = 0.3$ ; (4)  $f = 0.2$ ; (5)  $f = 0.15$ ; (1') dashed line; enlarged  $K/S$  for a sphere  $f = 1$ . (d) (continuous blue line) Calculated  $K/S$  for a distribution of shapes of Au NPs. (B) Histogram of the distribution of shape of gold NPs (aspect ratio  $f$ ).

If we assume independent absorption and scattering by the Au and TiO<sub>2</sub> particles,  $K$  and  $S$  are proportional to the number of particles and can be expressed as<sup>43</sup>

$$K_p = 2N_p C_{\text{abs}}^p \quad (4)$$

$$S_p = \frac{3}{4} N_p C_{\text{sca}}^p (1 - g) \quad (5)$$

where  $p = \text{Au or TiO}_2$ ,  $N_p$  is the total number of Au or TiO<sub>2</sub> particles per unit volume (number densities).  $C_{\text{abs}}^p$  is the absorption cross-section of the gold NPs (respectively TiO<sub>2</sub> grains), and the factor 2 in eq 4 comes from averaging over the trajectories.  $C_{\text{sca}}^p$  is the scattering cross-section of the Au NPs or TiO<sub>2</sub> grains. Here  $g$  is an anisotropy factor defined as the average value of the cosine of the scattering angle; for the case of very small particles, the scattering is symmetric with respect to the forward and back scattered directions, thus  $g$  reduces to zero.

Since the Au and TiO<sub>2</sub> particles are small with respect to the incident wavelength, one can use the quasi-static approximation (which neglects the retardation effects) to calculate the cross sections,  $C_{\text{abs}}^p$  and  $C_{\text{sca}}^p$ . In the case of TiO<sub>2</sub> grains that display some variety in sizes and rather rounded shapes, the averaging of the cross-section in all orientations has been approximated

by using the cross-section of spheres with an average radius. On the contrary, the plasmon resonance of the Au NPs is strongly dependent on their shape, and as indicated above, they have been considered as oblate spheroids with the revolution axis perpendicular to the surface of the TiO<sub>2</sub> substrate, which is an adequate model for small metal nanoparticles grown on a substrate.<sup>44–47</sup> Consequently, their shape depends on only one parameter, the aspect ratio defined by  $f = c_{\text{Au}}/a_{\text{Au}}$  where  $c_{\text{Au}}$  is the half-revolution axis and  $a_{\text{Au}}$  the half axis of the two other degenerate directions ( $f = c_{\text{Au}}/a_{\text{Au}} = 1$  for a sphere,  $f = c_{\text{Au}}/a_{\text{Au}} < 1$  for a flat (oblate) spheroid and  $f = c_{\text{Au}}/a_{\text{Au}} > 1$  for an elongated (prolate) spheroid). The absorption and scattering cross sections can be written as a function of the polarizabilities  $\alpha$  of the particles

$$C_{\text{abs}}^p = \frac{2\pi n_m}{\lambda} \text{Im}\alpha_p \quad (6)$$

$$C_{\text{sca}}^p = \frac{8\pi^3 n_m^4}{3\lambda^4} |\alpha_p|^2 \quad (7)$$

where  $\lambda$  is the wavelength of light in vacuum and  $n_m$  is the index of refraction of the embedding medium, given by  $n_m = (\epsilon_m)^{1/2}$ . In the present case, both the TiO<sub>2</sub> particles and the Au NPs supported on TiO<sub>2</sub> are in gas, whose dielectric function  $\epsilon_m$  is equal to 1. The TiO<sub>2</sub> particles are approximated as spheres, and in SI units, the polarizability reads as

$$\alpha_{\text{TiO}_2} = 4\pi a_{\text{TiO}_2}^3 \frac{\epsilon_{\text{TiO}_2} - \epsilon_m}{\epsilon_{\text{TiO}_2} + 2\epsilon_m} \quad (8)$$

where  $a_{\text{TiO}_2}$  is the radius of the TiO<sub>2</sub> spheres and  $\epsilon_m = 1$ . The titanium dioxide used in this study contains different proportions of rutile and anatase, which can be estimated to be around 30 and 70% respectively (see Experimental Section), both with an anisotropic uniaxial crystalline structure, therefore both with ordinary and extraordinary indices of refraction. Since the particles of anatase and of rutile are randomly oriented in the sample, we used in the following an average value (both in orientation and composition) of the dielectric functions of TiO<sub>2</sub>.<sup>48,49</sup>

The polarizability along one of the three principal perpendicular axes  $i$  of an unsupported ellipsoidal gold particle is given by<sup>33,50–52</sup>

$$\alpha_{\text{Au}}^i = 4\pi a_{\text{Au}}^2 c_{\text{Au}} \frac{1}{3} \frac{\epsilon_{\text{Au}} - \epsilon_m}{\epsilon_m + (\epsilon_{\text{Au}} - \epsilon_m)L_i} \quad (9)$$

where  $L_i$  is the depolarization factor along direction  $i$ . For gold particles supported on larger particles of TiO<sub>2</sub> (Figure 2A), the interaction of the polarized gold ellipsoids with the substrate can be described within the quasistatic image model<sup>44</sup> in terms of image charges within a planar substrate. Since the image charges are highly localized and lie very close to the interface, it has been shown previously that their highly inhomogeneous field induces back multipolar charge distributions in the particle.<sup>53</sup> All this causes a small red shift of the dipolar resonance and induces additional weak multipolar resonances besides the main dipolar one.<sup>39,40,52–55</sup> It has been shown that the treatment of this problem using a multipolar expansion in spheroidal

coordinates leads to a very fast numerical convergence; the so-called spheroidal dipolar approximation, which corresponds to keep up only the dipolar term in the multipolar expansion in spheroidal coordinates, already gives satisfying results.<sup>53,56</sup> With this approximation, eq 9 can still be used, but with modified depolarization factors  $L_i^{\text{mod}}$  given in ref 53, which account for the interaction with the substrate, and differ for electric fields parallel and perpendicular to the substrate. Using this approach, we calculate the modified polarizabilities  $\tilde{\alpha}_{\text{Au}}^i$  for the supported Au NPs. Since the gold particles are randomly oriented, we performed an orientational average by taking the mean of the polarizability over the three perpendicular directions, x, y and z,

$$\tilde{\alpha}_{\text{Au}}^{\text{Aver}} = \frac{1}{3}(\tilde{\alpha}_{\text{Au}}^x + \tilde{\alpha}_{\text{Au}}^y + \tilde{\alpha}_{\text{Au}}^z) \quad (10)$$

where z is the direction perpendicular to the surface of the TiO<sub>2</sub> substrate.

The dielectric function of gold,  $\epsilon_{\text{Au}}$  used in eq 9 has been taken from ref 37 but was modified with respect to bulk gold to take into account the electron scattering at the surface of small gold particles whose size is smaller than the electron mean free path in bulk  $l_{\text{bulk}}$ , equal to 12.8 nm.<sup>37</sup> One can write<sup>57–59</sup>

$$\epsilon_{\text{Au}}^{\text{mod}}(\omega) = \epsilon_{\text{Au}}^{\text{bulk}}(\omega) + \frac{\Omega_p^2}{\omega(\omega + i\tau_{\text{bulk}}^{-1})} - \frac{\Omega_p^2}{\omega(\omega + i\tau_{\text{mod}}^{-1})} \quad (11)$$

where

$$\Omega_p = \left( \frac{Ne^2}{\epsilon_0 m} \right)^{1/2} \quad (12)$$

is the Drude plasma frequency of the “free” or conduction s-p electrons in gold, that is, the value of the plasma frequency that does not take into account the screening due to the “bound” electrons, that is, the effect of the interband transitions. Here  $N$  is the density of conduction electrons,  $e$  is their charge, and  $m$  is their effective mass, and we are using SI units. For gold,  $\hbar\Omega_p = 9.04$  eV.<sup>37</sup>  $\tau_{\text{mod}}$  denotes the relaxation time of the free electrons in the Au NPs. It differs from its value  $\tau_{\text{bulk}}$  in gold bulk, because of the scattering of the conduction electrons at the surface of the NP, which reduces their mean free path  $l_{\text{mod}}$  ( $= v_{\text{Fermi}}\tau_{\text{mod}}$ ). For Au nanospheres, the following expression is often used<sup>34,59</sup>

$$l_{\text{mod}}^{-1} = l_{\text{bulk}}^{-1} + \frac{A}{R} \quad (13)$$

where  $R$  is the radius of the spheres and  $A$  is a phenomenological parameter, whose value ranges between about 0.1 and 1.5, depending on the theories describing the PR in a particle, and on the experiments. In our case of oblate spheroids, the best fitting of the experimental curve was obtained for  $A = 0.4$ . For the value of  $R$ , we used the average of the half-axes  $2/3a_{\text{Au}} + 1/3c_{\text{Au}}$ , where  $a_{\text{Au}}$  is taken equal to 2 nm, which corresponds approximately to the average value observed in Figure 2 ( $2a_{\text{Au}} = 4$  nm).

The combination of eqs 1–13 allows us to obtain the theoretical  $K/S$  curves for given shapes of Au particles. The number densities  $N_{\text{TiO}_2}$  and  $N_{\text{Au}}$  that appear in eqs 4 and 5 are equal to the filling fractions  $X_{\text{TiO}_2}$  and  $X_{\text{Au}}$  of each constituent in the powder (mixture of TiO<sub>2</sub> grains, of Au NPs and of gas), divided by the average volume of the corresponding particles,  $4/3 \pi a_{\text{TiO}_2}^3$  and  $4/3 \pi a_{\text{Au}}^2 c_{\text{Au}}$ , respectively. A combination of eqs 4 to 9 shows that  $K/S$  is proportional to the ratio of the filling fractions  $X_{\text{Au}}/X_{\text{TiO}_2}$ , (equal to 0.8%, see Experimental Section), divided by the volume of the TiO<sub>2</sub> grains; it does not depend on the size of the Au NPs, or on the compactness of the powder. The only indirect dependence on the size of the Au NPs is through the relaxation time in the dielectric function of gold (eq 11). The radius  $a_{\text{TiO}_2}$  of the TiO<sub>2</sub> grains is here an adjustable parameter which allowed us to fit the intensity of the experimental  $K/S$  curve. The best fit corresponds to  $a_{\text{TiO}_2} = 39$  nm. It is larger than the average size of individual TiO<sub>2</sub> particles seen in the TEM picture of Figure 2A ( $2a_{\text{TiO}_2} = 20$ –30 nm), which can be explained by some agglomeration of TiO<sub>2</sub> crystals, leading to an increase of its diffusion power. It is worth pointing out that in the visible range, the absorption of titanium dioxide is much smaller than the one of the Au NPs, that is,  $K_{\text{TiO}_2} \ll K_{\text{Au}}$  (eq 3). Moreover, as the Au NPs are about ten times smaller than the TiO<sub>2</sub> grains, and as scattering  $S$  varies as the sixth power of the linear size (eqs 7 and 8), light scattered by the Au NPs is negligible with respect to that scattered by TiO<sub>2</sub>, that is,  $S_{\text{TiO}_2} \gg S_{\text{Au}}$ . Moreover,  $S_{\text{TiO}_2}$  can be shown to have, in the visible range, almost no spectral dependence. Consequently, the measured  $K/S$  corresponds essentially to the absorption by the Au NPs.

The curves numbered from 1 to 5 in Figure 5A are the simulations of the  $K/S$  spectra for a catalyst, which would be constituted by NPs with a single shape, that is, a single aspect ratio  $f$ . The total amount of Au used to calculate the  $K/S$  curves of every aspect ratio has been taken equal to the actual amount, and every curve has been divided by a factor of 6, for the clarity of the figure. All the calculated plasmon resonance bands are narrower than the experimental one (Figure 5A, curve c). In the case of spheres ( $f = 1$ ), the calculated  $K/S$  spectrum shows a bandwidth smaller by a factor of about 2 to 3 than the experimental one (Figure 5A, curves 1 and 1'). For flatter particles, the resonance band shifts to longer wavelengths then broadens and increases in intensity. This increase comes partly from parameter  $S$ , dominated as indicated above by the scattering of TiO<sub>2</sub>, which varies as  $1/\lambda^4$  (eqs 5 and 7). Thus, the variation of  $K/S$  as  $\lambda^4$  leads in our DDRS measurements to a higher sensitivity to the flat Au particles displaying a resonance at long wavelengths, than to the round particles with resonance at short wavelengths. None of the calculated curves reported in Figure 5A fits the experimental spectrum. Consequently, a distribution of particle shapes has to be taken into account. Rather than using an analytical distribution (like a Gaussian distribution, or a log-normal distribution), which does not necessary provide a satisfying description of the real sample, an ad-hoc shape distribution was determined to fit the experimental spectrum; such a procedure has been recently successfully proposed in the case of Au nanorods.<sup>60</sup> For all aspect ratios  $f$ , we used  $a_{\text{Au}} = 2$  nm and  $c_{\text{Au}} = fa_{\text{Au}}$ , and the corresponding number densities  $N_{\text{Au}}(f)$  were fitted in order that the final result (curve d) reproduces well the experimental curve (c). Figure 5B reports the so-determined shape distribution. The particle shapes lie between spheres ( $f = 1$ ) and oblate spheroids with an aspect ratio  $f = 0.15$ , with a maximum centered at  $f = 0.5$  and an average aspect ratio  $f = 0.55$ . A shoulder in the distribution is

visible around  $f = 0.2$ , which could indicate the existence of a family of very flat particles, as discussed below. It has to be outlined that other distributions of shapes, although not very different from the present one but with the same shoulder around  $f = 0.2$ , enables us to fit satisfactorily the experimental  $K/S$ . The reason is double. First, the resonance is broad whatever the shape, thus the resonances of particles of different shapes overlap each with the others; second, for  $f \geq 0.6$ , the position of the resonance is almost unchanged and centered between 520 and 535 nm. One can see in Figure 5A that the calculated curve is in excellent agreement with the experimental one for wavelengths above 530 nm. The tail of the resonance observed at long wavelengths is explained by the existence of a relatively small number of very flat particles ( $f \leq 0.2$ ). Comparing calculated spectra 1 to 5, it can be seen that the spectrum that gives the maximum of absorbance at the shortest wavelengths is the one corresponding to spherical particles ( $f = 1$ ). The intensity of the measured signal below 530 nm, likely due also to plasmon resonances, cannot be fitted within the present model. The explanation is likely related to the actual profile of the electron distribution at the particle surface. Within the so-called jellium model based on the density functional theory, which gives a realistic description of the surface plasmons in metals,<sup>61</sup> it has been shown that the spill out of the free-electron distribution at the surface of the NPs can lead to a blue shift of the PR as large as 40 nm to smaller wavelengths in the case of Au NPs with radii smaller than 2 nm.<sup>35</sup> This effect is not included in the present calculation. Although it could be accounted for by an ad-hoc number of particles with a dielectric function different from the one of Au bulk, it will not be considered in our approach based on a classical model. The important issue here was not to get an exact description of the shape distribution set of Au NPs in the studied catalyst, but rather to use this description to determine the effect of the exposure to oxygen or to CO on the optical response of the catalyst.

#### 4. Relative Change of Diffuse Reflectance Induced by Oxygen Exposure

**4.1. Experimental Results.** In the second set of experiments the relative changes of diffuse reflectance were investigated upon exposure of Au/TiO<sub>2</sub> to different gases. All the measurements were performed at room temperature and atmospheric pressure by use of our homemade optical setup described in Figure 1. Figure 6 shows the differential diffuse reflectance spectrum (DDRS) of Au/TiO<sub>2</sub> and TiO<sub>2</sub> after gas switching from H<sub>2</sub> to O<sub>2</sub> and is defined by

$$\frac{\Delta R}{R} = \frac{R_{O_2} - R_{H_2}}{R_{H_2}}$$

The DDRS spectrum of TiO<sub>2</sub> without Au (curve b) is flat and shows no structure whereas that of Au/TiO<sub>2</sub> (curve a) presents an intense signal as large as 20%, which is therefore related to the Au NPs.

In this figure, one can see that  $\Delta R/R$  has a derivative-like shape with a slightly positive maximum around 520 nm, a negative minimum around 640 nm, and an inflection point around 550 nm. It is worth reminding that negative values of  $\Delta R/R$  correspond to an increased light absorption in the catalyst, and positive values to a decreased absorption. The negative peak at 640 nm should therefore correspond to an increase of the absorption caused by the excitation of the plasmon resonance

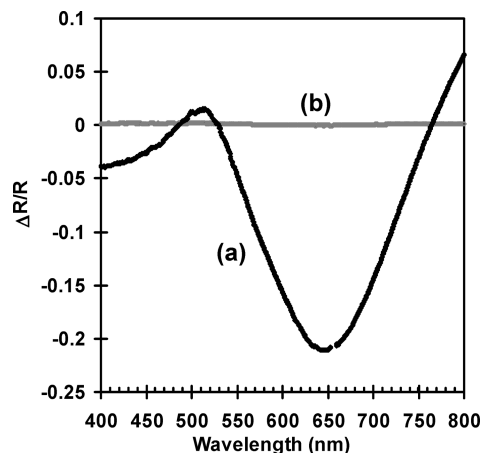


**Figure 6.** Differential diffuse reflectance spectrum  $\Delta R/R$  measured after exposing to oxygen the Au/TiO<sub>2</sub> catalyst previously exposed to hydrogen (curve a). The horizontal line (curve b) is the result of the same measurement performed on a TiO<sub>2</sub> sample without Au NPs.

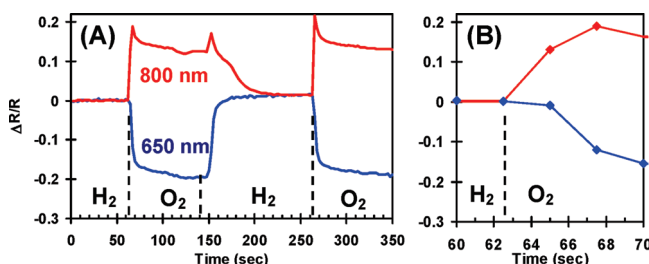


**Figure 7.** (A) Kinetics of the change in the DDR signal of Au/TiO<sub>2</sub> at two wavelengths, 650 nm (blue) and 800 nm (red); (B) Zoom between times 60 and 70 s at the first introduction of oxygen.

of the Au NPs in the presence of oxygen. At first sight, the general shape of the DDR spectrum can be explained by the shift of the plasmon resonance maximum from 550 nm for Au NPs in H<sub>2</sub> to 575 nm in O<sub>2</sub>, as seen also in Figure 3 and Figure 4 (curve b). The DDR spectrum induced by the modification of the diffuse reflectance of the sample upon O<sub>2</sub> atmosphere is stable and remains unchanged when the cell is flushed with pure He; the change is perfectly reversible and the DDRS comes back to a null spectrum when the cell is filled again with hydrogen. This can be seen clearly in Figure 7, which shows the kinetic evolution of the signal at two wavelengths, 650 and 800 nm, as a function of exposure to the different gases. The Au/TiO<sub>2</sub> sample was first exposed to hydrogen. Immediately after removal of hydrogen and introduction of oxygen, the DDR signal appears within a time scale of a few seconds after which curve a in Figure 6 is obtained. Subsequently, there is almost no change as long as the sample is maintained in oxygen atmosphere. When oxygen is removed and replaced by hydrogen, the signal comes back to its initial value, although less rapidly than during the switch from H<sub>2</sub> to O<sub>2</sub> (the kinetics will be discussed below).

**4.2. Theoretical Results.** The issue is now to determine the mechanism that causes this reversible modification of the optical response of the catalyst, when it is exposed to oxygen. Several hypotheses can be proposed, (a) adsorption of oxygen on the TiO<sub>2</sub> grains, modifying the dielectric function of TiO<sub>2</sub>; (b) formation of an oxide layer around the Au NPs; (c) adsorption of oxygen entities on the Au NPs with charge transfer from Au, yielding a change in the Drude plasma frequency  $\Omega_p$ ; (d) adsorption of oxygen entities on the Au NPs with change in the scattering of the “free” s-p electrons at the Au NP surface, yielding a modification of the Drude relaxation time  $\tau$ ; and (e)

change of shape of the Au NPs. In the following, each hypothesis will be examined, and the corresponding DDRS calculated and compared with the experimental spectrum.

**a. Change of the Dielectric Function of TiO<sub>2</sub>.** It has been proposed that in the reaction of CO oxidation over Au/TiO<sub>2</sub>, the surface of TiO<sub>2</sub> could be involved in the activation of oxygen, which would imply that a certain amount of oxygen would be adsorbed. Such effects can be taken into account by a change  $\Delta\epsilon_{\text{TiO}_2}$  of the dielectric function of TiO<sub>2</sub>, used in eq 8, which gives the polarizability of the TiO<sub>2</sub> grains. However, as this polarizability appears at the second power in the final calculation (eq 7), this leads to a negligible second order effect. We actually checked that a change as large as 10% in the dielectric function of TiO<sub>2</sub> leads to a featureless spectrum with an intensity five times smaller than the observed DDRS. In conclusion, even if oxygen adsorbs on TiO<sub>2</sub>, the effect would be too small to explain the spectral behavior of the experimental spectrum.

**b. Formation of an Oxide Layer on Gold Nanoparticles.** We examined the hypothesis of the formation of a thin layer of gold oxide on the Au NPs surface. Formation of surface oxide has been previously reported for gold surfaces exposed to atomic oxygen or oxygen plasma.<sup>22,62,63</sup> For instance, Au(core)/Au<sub>2</sub>O<sub>3</sub>(shell) structures with oxide shell thicknesses of about 0.7 nm were obtained when gold clusters were exposed to atomic oxygen.<sup>62</sup> In previous XAS studies performed on Au/TiO<sub>2</sub> and Au/Al<sub>2</sub>O<sub>3</sub> catalysts, only Au particles smaller than about 3 nm were found reactive to air, leading to oxidation of about 10% of the Au atoms, whereas larger particles did not seem to be oxidized.<sup>9,21</sup> On the other hand, few investigations have been performed on the optical properties of gold oxides. In an ellipsometric study of the formation of an anodic oxide layer on Au substrate with a positive applied electrochemical potential,<sup>64</sup> the thickness of the layer of oxide was experimentally determined equal to 0.33 nm and its complex index of refraction at  $\lambda = 632$  nm was found equal to  $n_{\text{ox}} = 3.3 + 1.35i$ . For comparison, the value for gold at the same wavelength is  $n_{\text{Au}} = 0.17 + 3.4i$ . This layer of gold oxide was identified as AuO oxide, which transformed into thicker film of Au<sub>2</sub>O<sub>3</sub> for more positive potentials. The use of this so-determined index of refraction for Au oxide will provide us the main trends of the effect of an actual oxide layer formed around the Au NPs. Using the shape distribution determined above (Section 3.2.c and Figure 5), we can describe the Au particles as core-shell oblate spheroidal particles, whose external Au layer (of thickness  $t_{\text{Au}}$ , chosen equal to the value of a compact (111) monolayer of gold, that is, 0.236 nm) is replaced by a Au oxide layer (of thickness  $t_{\text{shell}} = 0.33$  nm, with dielectric function  $\epsilon_{\text{shell}} = n_{\text{ox}}^2$ ). The geometrical parameters of the Au core and of the Au oxide shell are therefore  $a_{\text{Au}} - t_{\text{Au}}$  and  $c_{\text{Au}} - t_{\text{Au}}$ , and  $a_{\text{Au}} + t_{\text{shell}}$  and  $c_{\text{Au}} + t_{\text{shell}} - t_{\text{Au}}$ , respectively. Four effects are involved here. The volume of the metallic gold in the core is smaller than that in the nonoxidized particle, thus the intensity of the plasmon resonance should be lower; the metallic Au core for each oblate spheroidal particle becomes flatter ( $c_{\text{Au}}/a_{\text{Au}}$  ratio decreases), which should induce a red shift; the Au core is surrounded by a thin dielectric layer of oxide and not by gas, which should also induce a red shift, together with a damping of the plasmon resonance due to the imaginary part of the index of refraction of the Au oxide; the reduction of the core size induces also a reduction of the mean free path of the Au free electrons, therefore a reduction of the Drude relaxation time and a damping of the resonance.

The polarizability of a core-shell spheroid in vacuum along direction  $i$  with core and shell dielectric functions  $\epsilon_{\text{core}}$  and  $\epsilon_{\text{shell}}$  and a thickness  $t_{\text{shell}}$  for the shell is given by<sup>43</sup>

$$\alpha^i = V \left\{ (\epsilon_{\text{shell}} - \epsilon_{\text{emb}}) [\epsilon_{\text{shell}} + (\epsilon_{\text{core}} - \epsilon_{\text{shell}}) (L_i^{\text{core}} - \xi L_i^{\text{shell}})] + \xi \epsilon_{\text{shell}} (\epsilon_{\text{core}} - \epsilon_{\text{shell}}) \right\} / \left\{ [\epsilon_{\text{shell}} + (\epsilon_{\text{core}} - \epsilon_{\text{shell}}) (L_i^{\text{core}} - \xi L_i^{\text{shell}})] [\epsilon_{\text{emb}} + (\epsilon_{\text{shell}} - \epsilon_{\text{emb}}) L_i^{\text{shell}}] + \xi L_i^{\text{shell}} \epsilon_{\text{shell}} (\epsilon_{\text{core}} - \epsilon_{\text{shell}}) \right\} \quad (14)$$

where  $V$  is the total volume of the particle,  $L_i^{\text{shell}}$  and  $L_i^{\text{core}}$  are the depolarization factors of the inner and outer spheroids, respectively, and  $\xi$  is the ratio between the volume of the inner spheroid (the core) and  $V$

$$\xi = \frac{(a_{\text{Au}} - t_{\text{Au}})^2 (c_{\text{Au}} - t_{\text{Au}})}{(a_{\text{Au}} + t_{\text{shell}} - t_{\text{Au}})^2 (c_{\text{Au}} + t_{\text{shell}} - t_{\text{Au}})} \quad (15)$$

In the present case, we used the spheroidal dipolar approximation that describes the interaction of a spheroid with an uncoated substrate,<sup>65</sup> by replacing the depolarization factors used in eq 15 by the effective depolarization factors  $L_i^{\text{mod}}$  given in ref 53. We performed the calculation with two different values of the dielectric function of the gold oxide layer,  $\epsilon_{\text{shell}} = n_{\text{ox}}^2$ , where  $n_{\text{ox}} = 3.3 + 1.35i$  is the value reported above in ref 64, and  $\epsilon_{\text{shell}} = 1$ , which corresponds to an external layer of gold oxide without optical response. For the core, we used the same  $\epsilon_{\text{Au}}$  as above (eq 11).<sup>66</sup> Figure 8A compares the calculated spectra for  $\epsilon_{\text{shell}} = 1$  (curve b) and  $\epsilon_{\text{shell}} = n_{\text{ox}}^2$  (curve c) with the experimental spectrum a. When  $\epsilon_{\text{shell}}$  is taken equal to 1, the broad and intense positive maximum around 530 nm in the DDR spectrum is due to an increase of the reflectance, therefore to a global decrease of the absorption resulting from the lower amount of metallic gold in each particle. The negative values above 600 nm are due to a shift of the plasmon resonance toward longer wavelengths coming from the flattening of the metallic part of the particles. With  $\epsilon_{\text{shell}} = n_{\text{ox}}^2$ , spectrum c exhibits the same trend and the above-mentioned effects are even larger; in this case, the shift to longer wavelengths is due both to the flattening of the gold core and to the dielectric function of the shell. In both cases, the calculated effect is too large and does not reproduce the experimental results. Moreover, the experimental minimum around 640 nm is absent (except in the dashed blue curve (b') for  $\epsilon_{\text{shell}} = 1$ , that will be discussed below). Other values of  $\epsilon_{\text{shell}}$  have been tested, either real or complex, but all of them gave results quite different from the experimental spectrum. Consequently, the poor agreement between the calculated spectra and the experimental one allows us to rule out the hypothesis of the formation of an actual oxide layer on gold NPs. It is worth stressing the extreme sensitivity of the DDRS technique. The calculation shows that, even a slight modification of the gold particles, that is, the formation of one monolayer of oxide at the surface of the Au NPs, leads to a huge effect. To get a calculated spectrum with the same intensity as the measured one (but with a different shape), it would be necessary to have an oxide thickness equal to 0.04 nm, which has no physical meaning.

Despite the limitation of this simple calculation, it gives the main trend of the effect of the formation of an oxide gold layer around the Au NPs. Such an effect is clearly to be rejected. However, it does not exclude the adsorption of oxygen species,

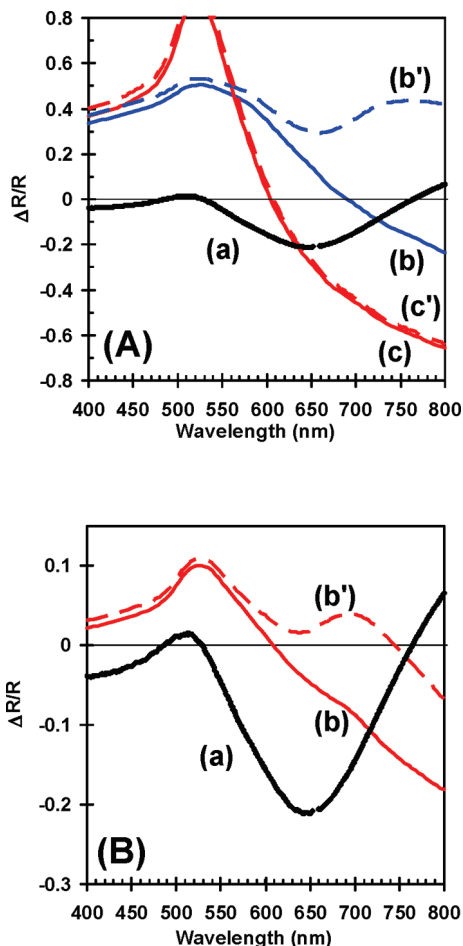


**Figure 8.** (A) (a) Experimental  $\Delta R/R$  spectrum of Au/TiO<sub>2</sub> (same as in Figure 6); (b) blue line, calculations performed with the oxide shell model, for  $\epsilon_{\text{shell}} = 1$ ; (c) red line, calculations performed with the oxide shell model, for  $\epsilon_{\text{shell}} = n_{\text{ox}}^2$ . (b') and (c'), dashed lines, similar calculations after removal of the plasmon resonance of the very flat NPs (see Section 4.2.d). (B) (a), Experimental  $\Delta R/R$  spectrum (same as in Figure 6); (b) calculations performed by changing the Drude parameter  $\tau$  (using  $A = 0.6$  instead of  $A = 0.4$ ); (b') dashed line, similar calculations after removal of the plasmon resonance of the very flat NPs (see Section 4.2.d).

which would modify only very slightly the optical response of the outer layer of Au. Such effects are examined in the next sections.

**c. Change of the Relaxation Time of the Drude Electrons in the Au NPs.** It has been shown that the interaction of metal particles with adsorbed molecules, or with molecules of the embedding medium or of the support that are in contact with the particles, can induce a damping of the plasmon resonance, which is called the “chemical interface damping”.<sup>34</sup> It has been explained by the temporary transfer of hot electrons of the plasmon excitation to “affinity levels” of the molecules bound to the Au NPs. Residence times of these electrons ( $10^{-14}$  s) are large enough to disturb the phase coherence of the collective excitation, and therefore to broaden the plasmon resonance.<sup>59</sup> This effect can be described by an increase of the factor  $A$  in eq 13, which is related to the proportion of electrons scattered at the NP surface. The increase of  $A$  from 0.4 for Au NPs in hydrogen (see above) to 0.6 for Au NPs in oxygen, leads to curve b in Figure 8B. Its shape is still far from the experimental one, and results from the additional damping and broadening of the plasmon resonance, leading to a lower absorption around the maximum at 550 nm in  $K/S$ , that is, positive values in the

DDR spectrum, but to a stronger absorption at longer wavelengths in  $K/S$ , that is, negative values in the DDR spectrum. The use of larger  $A$  values gives spectra of the same shape as curve b with larger positive and negative values. The dashed curve b' will be discussed below. The disagreement with the experiment leads us to conclude that even if some chemical interface damping occurs because of the adsorption of oxygen this cannot be the main effect.

**d. Charge Transfer from the Au NPs.** Previous studies showed that exposure of supported gold catalysts to O<sub>2</sub> is expected to induce a transfer of electrons from the surface Au atoms to the oxygen species.<sup>9,10</sup> This can be taken into account in a simple way by considering that the density  $N$  of the Au free s-p electrons, involved in the plasmon resonance of the particles, is reduced. After eq 12, the Drude plasma frequency is therefore modified and reads

$$\Omega_p^{\text{mod}} = \left( \frac{(N - \Delta N)e^2}{\epsilon_0 m} \right)^{1/2} = \Omega_p \left( 1 - \frac{\Delta N}{N} \right)^{1/2} \quad (16)$$

where  $\Delta N$  is the decrease of the free electron density  $N$  due to the charge transfer. This induces a modification of the Au dielectric function, given by eq 11, where  $\Omega_p$  in the last term is replaced by  $\Omega_p^{\text{mod}}$ , and induces consequently a red shift of the surface plasmon in the particle.

We start again with the shape distribution determined in Section 3.2.c (Figure 5B), with the particles described by the parameters  $a_{\text{Au}} = 2$  nm and  $c_{\text{Au}} = f a_{\text{Au}}$ . The number of surface atoms in a particle depends on its aspect ratio  $f$ ; the ratio of surface to bulk atoms increases as  $f$  decreases. Considering that the charge transfer is proportional to the number of surface atoms, its effect will be therefore more important for the flatter particles (small  $f$ ). The best agreement with the experiment is obtained for an average charge transfer equal to 0.13 electron per surface atom. For instance, for a spherical particle of radius  $a_{\text{Au}} = 2$  nm, the values obtained are  $\Delta N/N = 4.6\%$  and  $\hbar\Omega_p^{\text{mod}} = 8.83$  eV, instead of  $\hbar\Omega_p = 9.04$  eV for gold bulk, and for an oblate spheroid with  $f = 0.4$ ,  $\Delta N/N = 9.7\%$  and  $\hbar\Omega_p^{\text{mod}} = 8.59$  eV. The result of the calculation is spectrum b in Figure 9A. Both the maximum around 500 nm and the fast decrease of the experimental differential reflectance between 500 and 600 nm are correctly reproduced, although the calculated spectrum still displays positive values at short wavelengths. The discrepancy above 650 nm will be discussed below. It is worth mentioning that another approach, the two-layer model, has been very successful for interpreting differential reflectance spectra measured on noble metal surface in electrolytes;<sup>67</sup> because of the charging of the surface by the applied bias, the surface layer was considered to have a different density of electrons, while the bulk remained unchanged. In our case of Au NPs, we checked this approach by using the core–shell model described above (eq 14), where the internal dielectric function is the one of bulk gold, and the external Au monolayer has a modified dielectric function with a reduced density of free electrons, given by a fixed charge transfer for every surface Au atom. The obtained results are very similar to the previous ones in Figure 9A and are not presented here. Our results can be compared to recent optical transmission experiments performed on sensors made of TiO<sub>2</sub> semiconductor thin films, doped with 10 nm Au NPs and prepared by sol–gel technique. A similar but smaller shift of the plasmon resonance was obtained when the film was exposed to H<sub>2</sub> or to CO in air at the temperature of 360 °C.<sup>68</sup> Although this system and the experimental conditions are quite

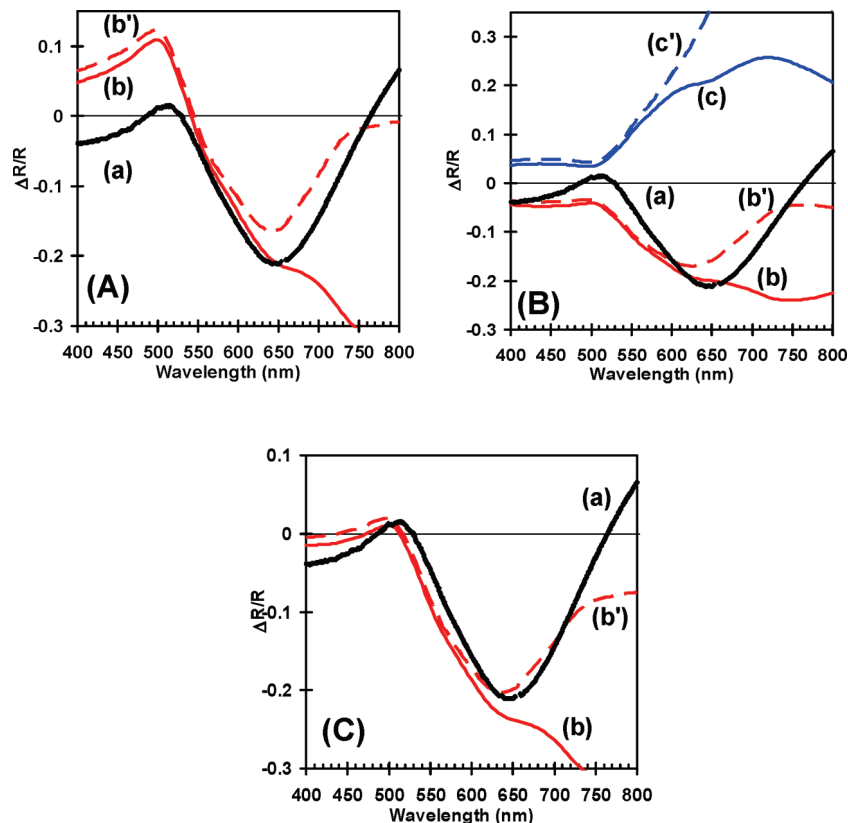


**Figure 9.** (A) (a) Experimental  $\Delta R/R$  spectrum of Au/TiO<sub>2</sub> (same as in Figure 6); (b) calculation with charge transfer.  $ct = 0.13$  electron per atom; (b'), dashed line, similar calculations after removal of the plasmon resonance of the very flat NPs (see Section 4.2.d). (B) (a) Experimental  $\Delta R/R$  spectrum (same as in Figure 6); (b) red line, calculation with flattening of NPs, factor  $x = 0.9$ ; (c) blue line, calculation with rounding of NPs, factor  $x = 1.1$ ; (b',c') dashed lines, similar calculations after removal of the plasmon resonance of the very flat NPs. (C) (a) Experimental  $\Delta R/R$  spectrum (same as in Figure 6); (b) combination of charge transfer ( $ct = 0.05$ ) and of change of shape ( $x = 0.92$ ); (b') dashed line, similar calculations after removal of the plasmon resonance of the very flat NPs.

different from ours, it is worth noticing that the authors interpreted also their data in terms of charge transfer from the Au NPs, leading also to a decrease of the bulk plasmon frequency, therefore a red shift of the plasmon resonance. However, the corresponding theoretical curves were not shown in ref 68 and the amount of charge transfer was not evaluated.

At this point, we have to discuss the experimental minimum around 650 nm and the positive slope for longer wavelengths (curve a in Figure 9A), leading even to positive DDR signal above 750 nm, which have not been reproduced by any of the previous calculations. The absolute  $K/S$  spectra measured in hydrogen and drawn in Figure 4 (curve c) shows a long absorption tail at long wavelengths, in addition to the resonance centered at 550 nm. The exposure of the catalyst to oxygen results in a red shift of the main resonance in  $K/S$  and an increase of the intensity of absorption, as well as a decrease of the absorption tail above 700 nm (curve b in Figure 4). In additional experiments not presented here, the diffuse reflectance of the catalyst has been monitored during the reduction of the “as-prepared” Au/TiO<sub>2</sub> sample and the progressive formation of the Au NPs in a hydrogen atmosphere. It showed that the PR develops in the following two steps: the first one is the main absorption around 550 nm, and the second one is the tail at longer wavelengths. This observation may indicate that the long and short wavelength plasmon resonances could be related to two kinds of Au NPs: one set of three-dimension particles as seen in the TEM pictures (Figure 2) leading to the PR at 550 nm, and a second set of possibly very flat particles, whose PR are located at longer wavelength. According to Figure 5A, the absorption around and above 700 nm would correspond to flat

particles with aspect ratios  $f$  smaller than 0.15. For NPs with dimension  $2a_{\text{Au}} = 4$  nm, this gives a short dimension  $2c_{\text{Au}} = 2fa_{\text{Au}} \leq 0.6$  nm, that is, about 3 monolayers or smaller. The presence of such very flat particles cannot be observed in our TEM pictures, and they are usually very difficult to be observed in TEM micrographs. A recent study using aberration-corrected scanning transmission electron microscopy, that is, a much more sophisticated TEM than ours, revealed the presence of 0.5 nm wide bilayer clusters in iron oxide-supported gold catalysts with about 10 atoms, which are presented as the actual active Au NPs for the oxidation in CO.<sup>69</sup>

The issue of the minimal size of the Au nanoparticles or clusters at which surface plasmon appears is the matter of active research.<sup>70–72</sup> The distinction between molecular-like optical absorption in very small clusters (a few tens of atoms), which involves intraband  $sp-sp$  transitions, and plasmon absorption in larger particles (more than 100 atoms), which involves collective motion of the  $sp$  electrons, is not clear. For instance, ligand-coated Au clusters with 25 atoms have been shown to display an asymmetric absorption centered at 700 nm with a tail up to 900 nm due to the  $sp-sp$  intraband transition of the 13 atoms (Au<sub>13</sub>) of the core of the cluster.<sup>71</sup> Similar absorption centered around 700 nm has been reported for coated Au<sub>13</sub> clusters.<sup>72</sup> In luminescence studies of gold clusters with 5 to 31 atoms, the free electrons are involved in a so-called “proto-plasmonic” intraband absorption, presented as “the small-size limit of the plasmon absorption within bulk metals”, and whose maximum absorption depends on the number of atoms.<sup>70</sup> Although the results obtained on ligand-stabilized Au clusters in solution cannot be directly transposed to the case of gold

particles on TiO<sub>2</sub>, it is possible that the long wavelength absorption observed here could be related to the presence of such supported Au clusters. In the following, if for the sake of brevity we continue to attribute this absorption at long wavelength to flatter particles, one has to keep in mind that it could be also arise from sp–sp intraband transitions in very small Au clusters. The important point is that the presently observed long wavelength absorption could be understood as the optical fingerprint of such Au clusters or of such Au very flat and small particles.

The kinetic experiments show that the short wavelength absorption and the long wavelength one evolve differently with respect to the exposure to oxygen, as illustrated in Figure 7, where the DDR signal evolution is drawn as a function of time at two different wavelengths,  $\lambda_{\min} = 650$  and  $\lambda_{\max} = 800$  nm.  $\lambda_{\min}$  corresponds to the minimum of the DDR spectrum and is related to the modification (mainly red shift) of the short-wavelength absorption resonance centered at 550 nm of the 3D particles, while  $\lambda_{\max}$  is related to the long-wavelength resonance of the “flattest” particles. The zoom in Figure 7B shows that after the introduction of oxygen, the signal at  $\lambda_{\max}$  immediately develops whereas the one at  $\lambda_{\min}$  is delayed for a couple of seconds. On the contrary, when oxygen is replaced by hydrogen (at time = 150 sec), the  $\lambda_{\min}$  signal is restored rapidly within a few seconds, while several tens of seconds are needed for the  $\lambda_{\max}$  signal. This indicates that the long wavelength resonance is more sensitive to the presence of oxygen and is easily damped but less easily restored.

Whatever the origin of the long wavelength resonance is, it is expected to be very sensitive to any effect due to the exposure to oxygen (charge transfer, change of shape, change in the bondings between atoms), and it could even be totally suppressed. To address this possible extreme sensitivity to oxygen of the long wavelength plasmon resonance in the very flat NPs or in the clusters, we took into account in the calculation based on the distribution of shapes, the suppression of the PR of the “flattest” NPs ( $f \leq 0.15$ ), induced by the exposure of the catalyst to oxygen. The result of this additional effect for the DDR spectrum is drawn in dashed line (curve b') in Figure 9A, within the analysis in term of charge transfer. The agreement with the experimental spectrum is now more satisfying in the whole spectral range despite some discrepancies and in particular the calculated positive values below 500 nm. Both the shape and the intensity of the experimental curve (a) are correctly reproduced. This very high sensitivity to oxygen of the “flattest” particles is in agreement with the observations made by Bondzie and coauthors, who studied the adsorption of O<sub>2</sub> on ultrathin gold particles supported on TiO<sub>2</sub>(110) and reported that the oxygen adsorption strength increases for the thinnest Au islands.<sup>73,74</sup> We also checked the effect of removing the PR of the “flattest” particles in the two previously proposed analyses, namely the formation of an oxide layer (dashed curves b' and c' in Figure 8A) and the modification of the relaxation time of the Drude electrons (dashed curve b') in Figure 8B. The results are not improved, and we can again rule out the corresponding hypotheses on the effect of oxygen.

**e. Change of Shape of the Au NPs Induced by Oxygen Adsorption.** It has been shown recently by environmental transmission electron microscopy in low pressure of gas that the shape of the Au particles could change slightly in the presence of a gas, becoming rounded up under oxygen and displaying facets under hydrogen.<sup>12</sup> This observation reveals the mobility of some surface atoms of the gold nanoparticles. As mentioned in Section 3.2, we do not explore in the present

approach the optical response of supported faceted particles, first because such calculations have not yet been reported in literature, and second because the distribution of shapes of such particles and their changes in shape would require a large number of adjustable parameters. In the analytical procedure we use, the change in shape of the spheroidal Au NPs induced by the exposure to oxygen can be taken into account by a simple parameter, giving the main trends of the change of the optical response of the system. We can consider either a flattening of all the particles, that is, a decrease of the aspect ratio  $f$ , or on the contrary an increase of  $f$ . From the previously determined shape distribution (Figure 5B), we replaced each aspect ratio  $f$  by  $xf$ , with  $x < 1$  for a flattening of the NPs, and  $x > 1$  for the opposite. Figure 9B shows the results obtained for  $x = 0.9$  (curve b) and  $x = 1.1$  (curve c). With an increased aspect ratio  $f$ , the calculated spectrum is completely opposite to the experimental one. On the contrary, the agreement is rather good for a flattening of the NPs. It must be noticed that negative values are obtained at short wavelengths, as observed in the experiment. Using in addition the same approach as in the previous section, that is, the suppression of the PR for the “flattest” particles with aspect ratio  $f$  smaller than 0.15, this leads to a qualitative good agreement with the experimental spectrum in the whole spectral range (curve b' in Figure 9B).

**4.3. Discussion of the Different Models.** The calculations have first shown that the absolute optical spectrum (curve c in Figure 5A) could not be fitted by considering a single particle shape, but required the use of a distribution of shapes based, for example, on oblate spheroidal shapes with various aspect ratios  $f$  (Figure 5B). This is an important fact that cannot be easily approachable by electron microscopy. The second important information is given by the kinetics experiment of switching gas, O<sub>2</sub>/H<sub>2</sub> (Figure 7), which revealed that the “flattest” Au particles are more sensitive to gas exchange. Indeed the kinetics of change of the DDR signal is faster at  $\lambda = 800$  nm than at 650 nm. Concerning the DDRS measurements (Figures 8 and 9), the results of the calculations using different models to reproduce the effect of adsorption of oxygen show that several of them can be excluded:

(i) A modification of the TiO<sub>2</sub> substrate has no visible effect on the DDR spectrum.

(ii) The presence of an oxide layer surrounding the Au NPs can be excluded, as the calculated curves have a very different shape than the experimental one.

(iii) The modification of the relaxation time of the Drude electrons resulting from interaction with adsorbed oxygen (“chemical interface damping”) cannot explain alone the experimental results, although it can have some influence.

On the other hand, the calculations show that the suppression (or at least a very strong damping) of the PR of the “flattest” particles, which is located at long wavelengths, is likely occurring. Nevertheless, the two models that reproduce properly the experimental observation are the one involving charge transfer between Au particles and oxygen and the one leading to flattening of the particles in the presence of oxygen. In the former case, the calculated spectrum exhibits positive values at short wavelengths (curve b' in Figure 9A), which are not observed experimentally (curve a). In the latter one, the shape of the spectrum at short wavelengths (curve b' in Figure 9B) with the positive maximum at 520 nm is not well reproduced (curve a). It is clear that both models are not exclusive; the change of shape of the particles (their flattening) is a strong evidence of direct adsorption of oxygen species on the Au NPs in agreement with environmental TEM.<sup>12</sup> This adsorption is

expected to be accompanied by charge transfer. Combining both models, that is, change of shape and charge transfer, leads to a very good agreement with experiment, except for wavelengths above 750 nm (curve b' in Figure 9C); the best fitting has been obtained with the parameters  $x = 0.92$  and  $ct = 0.05$  electron and when the PR for the "flattest" particles ( $f \leq 0.15$ ) has been removed.

These results show very conclusively that the adsorption of oxygen species on the Au NPs supported on TiO<sub>2</sub> induces a charge transfer from gold to oxygen, accompanied most likely by a flattening of the NPs. They show also that the flattest Au NPs (or Au clusters) are highly reactive to oxygen. However, these results do not bring information either on the activation of oxygen (resulting in possible dissociation of molecular oxygen or formation of O<sub>2</sub><sup>x-</sup> species, that is, with a weakened O–O bond), or about the adsorption sites of the oxygen species (on the Au particles or at the interface between Au NPs particles and the substrate). The oxygen active species involved in the catalytic oxidation of carbon monoxide could be molecularly adsorbed O<sub>2</sub> or atomically adsorbed oxygen. The latter hypothesis implies the dissociation of O<sub>2</sub> on the catalyst. Atomic oxygen has been demonstrated as reactive in CO oxidation.<sup>74–76</sup> However, the dissociation of O<sub>2</sub> on gold surfaces is not documented in the literature. Only a limited number of works reported the molecular adsorption of oxygen on model gold surface and gold nanoparticles<sup>4,19,63,77,78</sup> but some theoretical works indicate that low coordination sites (steps, edges, corners) of gold nanoparticles are suitable for molecular adsorption of oxygen.<sup>79–83</sup> The reactivity of CO and O<sub>2</sub> on anionic gold clusters Au<sub>n</sub><sup>-</sup> showed that the CO oxidation mechanism on these small gold clusters involves dioxygen species (superoxo O<sub>2</sub><sup>-</sup> or peroxo O<sub>2</sub><sup>2-</sup>)<sup>83–86</sup> rather than atomic oxygen and that the oxygen adsorption takes place via the charge transfer from the gold clusters to the antibonding  $\pi^*$  orbitals of O<sub>2</sub>.<sup>84,85</sup> Our interpretation in term of charge transfer from gold to the oxygen species which could be adsorbed at the surface of the Au NPs is in agreement with these works. It is also in agreement with experimental observations by use of XANES experiments. In a XANES study on Au/TiO<sub>2</sub> catalyst prepared in the same way but with Au particles with smaller average size than in the present paper, some of us found that the smallest particles are the more "reactive" toward oxygen.<sup>10,23</sup> More precisely, evidence was reported for "activated gold–oxygen complexes" at the surface of 1.7 nm Au NPs. It was suggested that the effect of these complexes could be a "depletion of the Au d-band in otherwise essentially metallic gold clusters. In the present approach, we consider a depletion of the sp conduction electrons with unchanged d-bands. It is possible that both effects occur, but that XANES mainly probes the changes of the Au d-bands, while the plasmon resonance mainly probes the changes in the sp conduction band. It can be also noticed that the counting of electrons in the different bands is not an easy issue, because of the non-negligible hybridization of the s, p, and d electrons in bulk Au as well in Au NPs; for instance, it has been shown from NEXAFS experiments and from calculations that some electron transfer occurs from the d-bands and the s-bands to the p-bands, and that the intensity of this transfer depends on the size of the Au NPs.<sup>87</sup>

### 5. Relative Change of the Diffuse Reflectance Induced by CO Exposure and by CO/O<sub>2</sub> Exposure

We also investigated the exposure of the Au/TiO<sub>2</sub> catalyst to CO. CO seems to have an effect very similar to the one of hydrogen, since switching gas from CO to O<sub>2</sub> gives spectra with

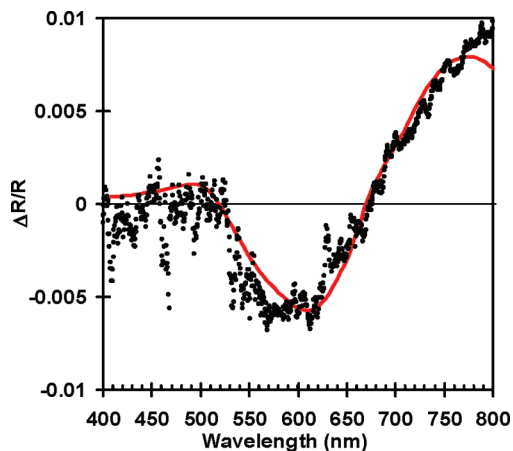


**Figure 10.** (a) Black dots, experimental differential diffuse reflectance spectrum  $\Delta R/R$  of Au/TiO<sub>2</sub> measured after exposing to CO the catalyst previously exposed to hydrogen; (b) continuous red line: combination of charge transfer with  $ct = 0.002$  and of flattening of Au NPs with  $x = 0.9975$ .

the same shape as the one drawn in Figure 6 (not shown here). In fact, effect of H<sub>2</sub> and of CO are not exactly the same; when switching from H<sub>2</sub> to CO, a small but visible effect is obtained (spectrum drawn with black dots in Figure 10). The shape of the spectrum with CO resembles the one with O<sub>2</sub> (spectrum a in Figure 6), but its intensity is 40 times smaller (for this reason, it is noisy). Comparison with the calculations presented in Figures 8 and 9 shows that the interpretation is likely the same as in the case of exposure to oxygen. Figure 10 reports the best result of calculation (red continuous curve), when considering a combination of the charge transfer and the flattening of the particles with the following parameters  $ct = 0.002$  and  $x = 0.9975$ . As done previously in the case of exposure to oxygen, the resonance of the "flattest" particles has been reduced (but in the present case not completely suppressed); the intensity of the PR for the particles defined by  $f \leq 0.16$  has been reduced by 7%, while the intensity of the PR for the particles defined by  $f = 0.12$  was reduced by 57%. It permits us to correctly reproduce the positive increase of the DDR signal above 700 nm. The theoretical curve reproduces very well the experimental spectrum. These results agree with previous studies. The adsorption of CO on the low-coordination sites of gold nanoparticles is indeed well documented in the literature.<sup>88–91</sup> A charge transfer from the gold nanoparticles to the adsorbed CO molecule was also found in the XANES studies previously reported<sup>9,10</sup> and was assigned to electron back-donation into the antibonding orbitals of CO, although the charge transfer between the d-band of gold and CO was stronger than with oxygen. Again, the electronic levels examined through UV–visible (sp bands) are different than those examined in XANES (d-band), and the hybridization between s, p, and d electrons prevents a straight comparison between these results.

### 6. Conclusion

The optical properties of Au/TiO<sub>2</sub> powder catalyst were investigated by means of diffuse reflectance spectroscopy. The observed intense absorption band centered at 550 nm is shown to be due to the excitation by light of plasmon resonances in the Au nanoparticles supported on the TiO<sub>2</sub> nanocrystals. Using an adequate model for describing the diffuse reflectance spectra, the shape and location of the absorption band could be interpreted by the distribution of shapes of Au NPs with a 4 nm average size. Most of the particles are three-dimensional

flat particles and can be modeled as oblate spheroids with an average aspect ratio centered around 0.5. The change of diffuse reflectance upon exposure to O<sub>2</sub> was real-time monitored by use of a highly sensitive homemade spectrometer. The differential diffuse reflectance spectra display derivative-like shapes due to the modification of the plasmon resonance of the NPs induced by the exposure to oxygen. Using this approximation for the oblate spheroidal shape of the Au NPs, several models based on reasonable hypotheses were examined in order to reproduce the experimental data. They enabled us to conclude that oxygen actually adsorbs on the Au NPs supported on the TiO<sub>2</sub> substrate, without formation of gold oxide. This adsorption induces a small charge transfer from gold to the oxygen species (about 0.05 electron per Au surface atom) as well as a slight flattening of the particles (around 8% decrease of the average aspect ratio). The exposure of the catalyst to CO, beforehand placed in hydrogen, leads to a similar but much smaller effect. A detailed analysis of the differential diffuse reflectance spectra and of the kinetics of their change upon exposure to the gases revealed the probable presence of two sets of nanoparticles, a majority that are flattened tridimensional NPs, and a minority that react more extensively with oxygen, and are either very flat, almost two-dimensional, NPs with an aspect ratio lower than 0.2 or clusters with a small number of atoms.

**Acknowledgment.** We would like to acknowledge illuminating discussion with Ignacio Garzon and with Mady Elias. This work has been partially supported by the French National Agency (ANR) in the frame of its Nanoscience Program (PNano, Project Reactgold No. ANR-07-NANO-024-01) and by the Consejo Nacional de Ciencia y Tecnología (Mexico) through Project No. 82073.

## References and Notes

- (1) Bond, G. C.; Louis, C.; Thompson, D. *Catalysis by Gold*; Imperial College Press: London, 2006; Vol. 6.
- (2) Haruta, M. *Nature* **2005**, *437*, 1098.
- (3) Kung, M. C.; Davis, R. J.; Kung, H. H. *J. Phys. Chem. C* **2007**, *111*, 11767.
- (4) Meyer, R.; Lemire, C.; Shaikhutdinov, S. K.; Freund, H. J. *Gold Bull.* **2004**, *37*, 72.
- (5) Hammer, B.; Norskov, J. K. *Nature* **1995**, *376*, 238.
- (6) Chen, M. S.; Goodman, D. W. *Science* **2004**, *306*, 252.
- (7) Liu, Z. P.; Gong, X. Q.; Kohanoff, J.; Sanchez, C.; Hu, P. *Phys. Rev. Lett.* **2003**, *91*, 266102.
- (8) Hernandez, N. C.; Sanz, J. F.; Rodriguez, J. A. *J. Am. Chem. Soc.* **2006**, *128*, 15600.
- (9) van Bokhoven, J. A.; Louis, C.; T. Miller, J.; Tromp, M.; Safonova, O. V.; Glatzel, P. *Angew. Chem.* **2006**, *45*, 4651.
- (10) Weiher, N.; Beesley, A. M.; Tsapatsaris, N.; Delannoy, L.; Louis, C.; van Bokhoven, J. A.; Schroeder, S. L. M. *J. Am. Chem. Soc.* **2007**, *129*, 2240.
- (11) Kotobuki, M.; Leppelt, R.; Hansgen, D. A.; Widmann, D.; Behm, R. J. *J. Catal.* **2009**, *264*, 67.
- (12) Giorgio, S.; Cabie, M.; Henry, C. R. *Gold Bull.* **2008**, *41*, 167.
- (13) Jiang, P.; Porsgaard, S.; Borondics, F.; Kober, M.; Caballero, A.; Bluhm, H.; Besenbacher, F.; Salmeron, M. *J. Am. Chem. Soc.* **2010**, *132*, 2858.
- (14) Lopez, N.; Norskov, J. K. *J. Am. Chem. Soc.* **2002**, *124*, 11262.
- (15) Schubert, M. M.; Hackenberg, S.; van Veen, A. C.; Muhler, M.; Plzak, V.; Behm, R. J. *J. Catal.* **2001**, *197*, 113.
- (16) Haruta, M.; Daté, M. *Appl. Catal., A* **2001**, *222*, 427.
- (17) Ariei, S.; Mortin, F.; Renouprez, A. J.; Rousset, J. L. *J. Am. Chem. Soc.* **2004**, *126*, 1199.
- (18) Franceschetti, A.; Pennycook, S. J.; Pantelides, S. T. *Chem. Phys. Lett.* **2003**, *374*, 471.
- (19) Stiehl, J. D.; Kim, T. S.; McClure, S. M.; Mullins, C. B. *J. Am. Chem. Soc.* **2004**, *126*, 1606.
- (20) Stiehl, J. D.; Kim, T. S.; McClure, S. M.; Mullins, C. B. *J. Am. Chem. Soc.* **2004**, *126*, 13574.
- (21) Miller, J. T.; Kropf, A. J.; Zha, Y.; Regalbutto, J. R.; Delannoy, L.; Louis, C.; Bus, E.; van Bokhoven, J. A. *J. Catal.* **2006**, *240*, 222.
- (22) Ono, L. K.; Cuenya, B. R. *J. Phys. Chem. C* **2008**, *112*, 4676.

- (23) Weiher, N.; Bus, E.; Delannoy, L.; Louis, C.; Ramaker, D. E.; Miller, J. T.; van Bokhoven, J. A. *J. Catal.* **2006**, *240*, 100.
- (24) Zanella, R.; Giorgio, S.; Henry, C. R.; Louis, C. *J. Phys. Chem. B* **2002**, *106*, 7634.
- (25) Zanella, R.; Delannoy, L.; Louis, C. *Appl. Catal., A* **2005**, *291*, 62.
- (26) Zanella, R.; Giorgio, S.; Shin, C. H.; Henry, C. R.; Louis, C. *J. Catal.* **2004**, *222*, 357.
- (27) Kubelka, P. *J. Opt. Soc. Am.* **1948**, *38*, 448.
- (28) Curiel, F.; Vargas, W. E.; Barrera, R. G. *Appl. Opt.* **2002**, *41*, 5969.
- (29) As the obtained K/S ratio is large, it is out of the usual domain of validity of the Kubelka–Munk approximation, and a full theoretical treatment would be necessary to check if eq 2 is still perfectly valid.
- (30) Sosa, I. O.; Noguez, C.; Barrera, R. G. *J. Phys. Chem. B* **2003**, *107*, 6269.
- (31) Noguez, C. *J. Phys. Chem. C* **2007**, *111*, 3806.
- (32) Gonzalez, A. L.; Reyes-Esqueda, J. A.; Noguez, C. *J. Phys. Chem. C* **2008**, *112*, 7356.
- (33) Landau, L. D.; Lifshitz, E. M. *Electrodynamics of continuous media*; Pergamon Press: New York, 1960.
- (34) Kreibig, U.; Vollmer, M. *Optical Properties of Metal Clusters*; Springer: New York, 1994.
- (35) Palpant, B.; Prevel, B.; Lerme, J.; Cottancin, E.; Pellarin, M.; Treilleux, M.; Perez, A.; Vialle, J. L.; Broyer, M. *Phys. Rev. B* **1998**, *57*, 1963.
- (36) Myroshnychenko, V.; Rodriguez-Fernandez, J.; Pastoriza-Santos, I.; Funston, A. M.; Novo, C.; Mulvaney, P.; Liz-Marzan, L. M.; de Abajo, F. J. G. *Chem. Soc. Rev.* **2008**, *37*, 1792.
- (37) Johnson, P. B.; Christy, R. W. *Phys. Rev. B* **1972**, *6*, 4370.
- (38) Barrera, R. G.; Delcastillo-mussot, M.; Monsivais, G.; Villasenor, P.; Mochan, W. L. *Phys. Rev. B* **1991**, *43*, 13819.
- (39) Beitia, C.; Borensztein, Y.; Barrera, R. G.; Roman-Velazquez, C. E.; Noguez, C. *Physica B* **2000**, *279*, 25.
- (40) Beitia, C.; Borensztein, Y.; Lazzari, R.; Nieto, J.; Barrera, R. G. *Phys. Rev. B* **1999**, *60*, 6018.
- (41) Tiggesbaumker, J.; Koller, L.; Meiwesbroer, K. H.; Liebsch, A. *Phys. Rev. A* **1993**, *48*, R1749.
- (42) Borensztein, Y.; Deandres, P.; Monreal, R.; Lopezrios, T.; Flores, F. *Phys. Rev. B* **1986**, *33*, 2828.
- (43) Bohren, C. F.; Huffman, D. R. *Absorption and Scattering of Light by Small Particles*; Wiley: New York, 1998.
- (44) Yamaguchi, T.; Yoshida, S.; Kinbara, A. *Thin Solid Films* **1974**, *21*, 173.
- (45) Flores-Camacho, J. M.; Sun, L. D.; Saucedo-Zeni, N.; Weidinger, G.; Hohage, M.; Zeppenfeld, P. *Phys. Rev. B* **2008**, *78*, 085408.
- (46) Witkowski, N.; Borensztein, Y.; Baudot, G.; Repain, V.; Girard, Y.; Rousset, S. *Phys. Rev. B* **2004**, *70*.
- (47) Lazzari, R.; Renaud, G.; Revenant, C.; Jupille, J.; Borensztein, Y. *Phys. Rev. B* **2009**, *79*, 125428.
- (48) Jellison, G. E.; Modine, F. A.; Boatner, L. A. *Opt. Lett.* **1997**, *22*, 1808.
- (49) Jellison, G. E.; Boatner, L. A.; Budai, J. D.; Jeong, B. S.; Norton, D. P. *J. Appl. Phys.* **2003**, *93*, 9537.
- (50) Abeles, F.; Borensztein, Y.; Lopezrios, T. *Festkorperprobleme - Adv. Solid State Phys.* **1984**, *24*, 93.
- (51) Martin, D.; Creuzet, F.; Jupille, J.; Borensztein, Y.; Gadenne, P. *Surf. Sci.* **1997**, *377*, 958.
- (52) Martin, D.; Jupille, J.; Borensztein, Y. *Surf. Sci.* **1998**, *402*, 433.
- (53) Bobbert, P. A.; Vlioger, J. *Physica A* **1987**, *147*, 115.
- (54) Lazzari, R.; Renaud, G.; Revenant, C.; Jupille, J.; Borensztein, Y. *Phys. Rev. B* **2009**, *79*, 125428.
- (55) Lazzari, R.; Jupille, J.; Borensztein, Y. *Appl. Surf. Sci.* **1999**, *142*, 451.
- (56) Valamanesh, M.; Borensztein, Y.; Langlois, C.; Lacaze, E., unpublished.
- (57) Borensztein, Y.; Alameh, R.; Roy, M. *Phys. Rev. B* **1994**, *50*, 1973.
- (58) Cooper, B. R.; Ehrenrei, H.; Philipp, H. R. *Phys. Rev.* **1965**, *138*, A494.
- (59) Hovel, H.; Fritz, S.; Hilger, A.; Kreibig, U.; Vollmer, M. *Phys. Rev. B* **1993**, *48*, 18178.
- (60) Eustis, S.; El-Sayed, M. A. *J. Appl. Phys.* **2006**, *100*, 044324.
- (61) Liebsch, A. *Phys. Rev. B* **1993**, *48*, 11317.
- (62) Boyen, H. G.; Kastle, G.; Weigl, F.; Koslowski, B.; Dietrich, C.; Ziemann, P.; Spatz, J. P.; Riethmuller, S.; Hartmann, C.; Moller, M.; Schmid, G.; Garnier, M. G.; Oelhafen, P. *Science* **2002**, *297*, 1533.
- (63) Min, B. K.; Alemozafar, A. R.; Pinnaduwa, D.; Deng, X.; Friend, C. M. *J. Phys. Chem. B* **2006**, *110*, 19833.
- (64) Xia, S. J.; Birss, V. I. *J. Electroanal. Chem.* **2001**, *500*, 562.
- (65) The model proposed in ref 53 is valid for a spheroid made of one material. As no model has been reported for a core–shell spheroidal particle, we used the modified depolarization factors of simple spheroids given in ref 53.

- (66) It is also possible that the shell does not cover the region between the Au particle and the substrate. We are aware of this limitation of the model, but we do not think that this would change qualitatively our results.
- (67) Kotz, R.; Kolb, D. M. *Z. Phys. Chem.* **1978**, *112*, 69.
- (68) Buso, D.; Post, M.; Cantalini, C.; Mulvaney, P.; Martucci, A. *Adv. Funct. Mat.* **2008**, *18*, 3843.
- (69) Herzing, A. A.; Kiely, C. J.; Carley, A. F.; Landon, P.; Hutchings, G. J. *Science* **2008**, *321*, 1331.
- (70) Zheng, J.; Nicovich, P. R.; Dickson, R. M. *Annu. Rev. Phys. Chem.* **2007**, *58*, 409.
- (71) Zhu, M.; Aikens, C. M.; Hollander, F. J.; Schatz, G. C.; Jin, R. *J. Am. Chem. Soc.* **2008**, *130*, 5883.
- (72) Menard, L. D.; Gao, S. P.; Xu, H. P.; Twisten, R. D.; Harper, A. S.; Song, Y.; Wang, G. L.; Douglas, A. D.; Yang, J. C.; Frenkel, A. I.; Nuzzo, R. G.; Murray, R. W. *J. Phys. Chem. B* **2006**, *110*, 12874.
- (73) Bondzie, V. A.; Parker, S. C.; Campbell, C. T. *J. Vac. Sci. Technol., A* **1999**, *17*, 1717.
- (74) Bondzie, V. A.; Parker, S. C.; Campbell, C. T. *Catal. Lett.* **1999**, *63*, 143.
- (75) Stiehl, J. D.; Kim, T. S.; Reeves, C. T.; Meyer, R. J.; Mullins, C. B. *J. Phys. Chem. B* **2004**, *108*, 7917.
- (76) Kim, T. S.; Stiehl, J. D.; Reeves, C. T.; Meyer, R. J.; Mullins, C. B. *J. Am. Chem. Soc.* **2003**, *125*, 2018.
- (77) Stiehl, J. D.; Gong, J. L.; Ojifinni, R. A.; Kim, T. S.; McClure, S. M.; Mullins, C. B. *J. Phys. Chem. B* **2006**, *110*, 20337.
- (78) Choi, K. H.; Coh, B. Y.; Lee, H. I. *Catal. Today* **1998**, *44*, 205.
- (79) Xu, Y.; Mavrikakis, M. *J. Phys. Chem. B* **2003**, *107*, 9298.
- (80) Lopez, N.; Norskov, J. K. *J. Am. Chem. Soc.* **2002**, *124*, 11262.
- (81) Liu, Z.-P.; Hu, P.; Alavi, A. *J. Am. Chem. Soc.* **2002**, *124*, 14770.
- (82) Molina, L. M.; Rasmussen, M. D.; Hammer, B. *J. Chem. Phys.* **2004**, *120*, 7673.
- (83) Sanchez, A.; Abbet, S.; Heiz, U.; Schneider, W. D.; Häkkinen, H.; Barnett, R. N.; Landman, U. *J. Phys. Chem. A* **1999**, *103*, 9573.
- (84) Salisbury, B. E.; Wallace, W. T.; Whetten, R. L. *Chem. Phys.* **2000**, *262*, 131.
- (85) Stolcic, D.; Fischer, M.; Gantefor, G.; Kim, Y. D.; Sun, Q.; Jena, P. *J. Am. Chem. Soc.* **2003**, *125*, 2848.
- (86) Wallace, W. T.; Whetten, R. L. *J. Am. Chem. Soc.* **2002**, *124*, 7499.
- (87) van Bokhoven, J. A.; Miller, J. T. *J. Phys. Chem. C* **2007**, *111*, 9245.
- (88) Bollinger, M. A.; Vannice, M. A. *Appl. Catal., B* **1996**, *8*, 417.
- (89) Grunwaldt, J. D.; Maciejewski, M.; Becker, O. S.; Fabrizioli, P.; Baiker, A. *J. Catal.* **1999**, *186*, 458.
- (90) Minicò, S.; Scirè, S.; Crisafulli, C.; Visco, A. M.; Galvagno, S. *Catal. Lett.* **1997**, *47*, 273.
- (91) Mihaylov, M.; Knozinger, H.; Hadjiivanov, K.; Gates, B. C. *Chem.-Ing. -Tech.* **2007**, *79*, 795.

JP101248H